INTERNATIONAL JOURNAL OF CLIMATOLOGY
Int. J. Climatol. **32**: 2372–2386 (2012)
Published online 31 October 2011 in Wiley Online Library
(wileyonlinelibrary.com) DOI: 10.1002/joc.3398

RMetS
Royal Meteorological Society

A numerical study of the Urban Heat Island over Madrid during the DESIREX (2008) campaign with WRF and an evaluation of simple mitigation strategies

Francisco Salamanca,[a]* Alberto Martilli[a] and Carlos Yagüe[b]
[a] *CIEMAT (Research Centre for Energy, Environment and Technology), Madrid, Spain*
[b] *Dept. de Geofísica y Meteorología, Universidad Complutense de Madrid, Spain*

ABSTRACT: Nowadays, mesoscale meteorological models coupled to Urban Canopy Parameterizations (UCP) can be used to complement and interpret the information gathered from intensive meteorological campaigns on the behaviour of the Urban Boundary Layer (UBL). Moreover, the impact of the air conditioning (AC) systems on the air temperature, the relationships existing between energy consumption (EC) and meteorological conditions, and the evaluation of strategies to mitigate the Urban Heat Island (UHI) phenomenon can be evaluated using detailed UCP. In this work, a new UCP implemented in the Weather Research and Forecasting (WRF) model (version V3.2) has been tested over the city of Madrid using two different turbulent parameterisations of the Planetary Boundary Layer (PBL) under atmospheric conditions that were favourable for a large UHI. Two selected days were analysed coinciding with the Dual-use European Security IR Experiment (DESIREX) campaign that took place in the summer of 2008, and focused on Urban Heat Island (UHI) and Urban Thermography (UT) monitoring and assessment. For the two simulated days (30 June and 1 July) a high UHI intensity (5-6 °C) was observed and modelled. Numerical results for the surface air temperature and wind speed were compared against measurements showing a global satisfactory performance of the model. Some differences in the air temperature predictions were observed within the two turbulent schemes. Subsequently, the impact of the AC systems and the EC were evaluated for the simulated period. The heat fluxes coming from AC systems were responsible of an increase in the air temperature up to 1.5–2 °C in some dense urban areas. Effects of modifications in the roof albedo and building material properties reduced the total EC by 4.8 and 3.6%, respectively, affecting the intensity of the UHI. When AC systems were not ejecting the heat fluxes out in the atmosphere, the EC was reduced to 2.5%. Copyright © 2011 Royal Meteorological Society

KEY WORDS anthropogenic heat; energy consumption; mesoscale models; turbulent schemes; urban boundary layer; urban heat island; urban canopy parameterisations

Received 14 January 2011; Revised 19 September 2011; Accepted 9 October 2011

1. Introduction

In the last few decades, the development of mesoscale models (MMs) accompanied by an increasing number of meteorological campaigns have contributed notably to a better understanding of the complex processes (Oke, 1987; Arnfield, 2003) that occur in the urban boundary layer (UBL). At the beginning of the twentyfirst century the first urban canopy parameterisations (UCP) that model the mechanical and thermal impact of cities in MMs (e.g. Masson, 2000 ; Kusaka *et al*., 2001 ; Martilli *et al*., 2002 ; Kanda *et al*., 2005) were proposed. These important developments provided a more realistic physical description of the urban areas, and contributed to a better understanding of their impact on the lower atmosphere. Ever since then, a large number of urban areas have been investigated (e.g. Martilli *et al*., 2003; Lo *et al*., 2006; Lemonsu *et al*., 2009) showing the ability of the UCPs to reproduce the processes that take place in the UBL.

Among these processes, one of the most important is the Urban Heat Island (UHI) that indicates the higher temperature existing within cities compared to the surrounding rural areas. The UHI intensity is usually defined as the difference in air temperature between two observatories, the urban and the rural one. A fundamental component that increases the intensity of the UHI is the anthropogenic heat (AH) generated by human activities, besides the altered radiation and energy budget in built-up areas, mainly as a result of replacing natural surfaces by buildings and pavements with different thermal inertia (Landsberg, 1981). The sources of AH (sensible/latent) released into the atmosphere are associated with the energy consumption and can be classified into three principal sectors: industry, buildings, and transportation (Sailor, 2011). It is known that fundamental contributions of AH in the commercial/residential areas are due to energy use in buildings for heating,

* Correspondence to: F. Salamanca, Lawrence Berkeley National Laboratory (LBNL), 1 Cyclotron Road, MS90K, Berkeley, CA 94720.
E-mail: fsalamanca@lbl.gov

ventilation, and air conditioning (AC) systems. In the first urban parameterisations (e.g. Masson 2000; Martilli *et al*., 2002), the AH was not computed explicitly and coarse simplifications (e.g. keeping the indoor surface temperature of the buildings constant in time) were considered in the simulations. Alternatively, a source term of heat estimated from energy consumption databases was added to the atmospheric equations (Kusaka *et al*., 2001), without considering the real spatial variability of the energy consumption. One of the first studies where the AH (ejected by the AC systems into the atmosphere) was computed through an urban parameterisation, was the work of Kikegawa *et al*., (2003), who integrated a simple building energy model (BEM) in an UCP. In this work, the relationship between the outdoor temperature and the energy consumption was studied for the city of Tokyo, and the AC systems were responsible for an increase up to 1 °C(in average) in the outdoor temperature. The coupling between a BEM and an UCP offers a spread of new possibilities when they are integrated in an atmospheric model. The effect of the AC systems in the air temperature, the quantification of the AH and its impact on the UHI phenomenon, as well as the evaluation of energy consumption mitigation strategies are some examples of the features that can be investigated, thanks to this linkage. However, a handicap can appear when an UCP+BEM scheme is used to compute the AH given that these fluxes are strongly dependent of the urban parameters that describe the morphology of the city. The lack of an accurate dataset for these parameters could overestimate or underestimate the AH fluxes (Salamanca *et al*., 2011).

In the last few years, an important effort is being carried out in the USA (Ching *et al*., 2009) to provide detailed urban canopy parameters to improve the parameterisation of UBL processes. Continuing in this line, Salamanca *et al*. (2010a) developed a new BEM that accounts for: (1) the diffusion of heat through walls, roofs, and floors; (2) natural ventilation; (3) the radiation exchanged between indoor surfaces; (4) the generation of heat due to occupants and equipments; and (5) the consumption of energy due to the use of the air conditioning systems. BEM was coupled to an UCP (BEP, building effect parameterisation of Martilli *et al*., 2002) and tested off-line over the city of Basel (Salamanca and Martilli, 2010). This scheme (BEP+BEM) has been integrated in the public Weather Research and Forecasting (WRF) model (Skamarock *et al*., 2008) V3.2 release. The new BEP+BEM scheme was tested against measurements over the city of Houston (Texas, USA), and was able to produce reasonable estimations of energy consumption (EC) when a high-resolution urban canopy parameters dataset was used (Salamanca *et al*., 2011).

In the summer of 2008, the Dual-use European Security IR Experiment (DESIREX) campaign (see DESIREX final report, Sobrino *et al*., 2009), run by the European Space Agency (ESA) was carried out in the city of Madrid (Spain). An important aim of the campaign was to study the UHI in support to mitigation strategies and urban energy efficiency policies. In this paper, thanks to the availability of the measured data, the BEP+BEM scheme implemented in the WRFV3.2, has been tested over Madrid. The UHI in Madrid is known since decades (Yagüe *et al*., 1991). However, it has never been investigated numerically with a detailed UCP so far. Meteorological modelling studies over the region have been carried out in the last few years, but always focussing on air pollution episodes (e.g. Palacios *et al*., 2002). The aim of this work is twofold: on one hand, to evaluate the ability of the new BEP+BEM scheme to describe the surface air temperature and wind speed over the city of Madrid in summer conditions with two different turbulent schemes, and on the other hand, to evaluate some simple energy consumption mitigation strategies and their relationship with the UHI intensity.

In Section 2, a description of the studied area and experimental framework are displayed. In the first part of Section 3, the setup of the simulations is presented, and in the second part numerical results are analysed and compared against measurements. In Section 4, the UHI and numerical sensitive experiments relative to energy consumption mitigation strategies are presented, and finally in Section 5, conclusions and future work are pointed out.

2. DESIREX campaign

2.1. Madrid area

Madrid (Figure 1) is the capital and largest city of Spain. It is located in the central part of the Iberian Peninsula (40°25′N, 3°41′W) in a relatively flat area about 50 km southeast of the Spanish Central Ridge. A small valley crosses the city from north to south acting frequently as a channel for air masses from the cooler northern rural areas. The maximum elevation within the city is located in the northern part reaching about 700 m above sea level (a.s.l.), while the lower occurs at the Manzanares River, around 550 m. The population of the city is roughly 3.2 million and it has not undergone important changes since 1970, while the estimated population of the metropolitan area is 5.1 million, with a significant increase in the last decades. The urban areas span a total of 607 km^2. The coordinates of the centre of the tested area are 40°23′N and 3°43′W.

Madrid has a climate with cool winters, with temperatures that sometimes drop below 0 °C, and dry hot summers (the mean maximum temperature in July is 31.2 °C) with temperatures that can reach up to 40 °C in July and August (for more details, see Sobrino *et al*., 2009).

2.2. Experimental framework

The DESIREX campaign took place in the summer of 2008 from 23 June to 6 July. Significant measurements activities were carried out involving an important number of researchers and institutions. In this section, only the part used in this work relative to atmospheric measurements is described (for more details

Figure 1. Map of the SW of Europe with Madrid in the middle of the Iberian Peninsula (picture obtained from Google Earth).

see the final report of the campaign, Sobrino *et al.*, 2009). Figure 2 shows the location of the measurements deployed during the campaign. In Table I, the corresponding measurement sites and coordinates are indicated. The AS6, AS7, and FM1 sites are out of the map of Figure 2.

Wind directions, wind speed, solar radiation, relative humidity, atmospheric pressure, air temperature, and precipitations were measured during the campaign by the meteorological network of the city council of Madrid. The same city council and the Region of Madrid also operated an air quality network (Surveillance network in Table I) that measured wind speed, wind direction, air temperature, pressure, solar radiation, and precipitation. Other meteorological stations belonging to the Spanish Meteorological Agency (AEMET) were also included in the campaign.

3. WRF simulations

3.1. Numerical domain and setup of the simulations

Two summer days (high-pressure period) have been analysed, 30 June and 1 July 2008 (days of year, 182 and 183, respectively), coinciding with the most important development of the UHI. It is a typical summer synoptic situation, showing stability at high levels and very weak horizontal pressure gradients, resulting in clear skies with

Table I. Measurements sites and coordinates of the DESIREX campaign activities (source DESIREX final report).

Measurements	ID	Urban Class	Site	Latitude (N)	Longitude (W)	Altitude (m) asl
Radio-sounding	RS1	OUA	AEMET-Barajas	40° 27′ 15″	3° 32′39″	582
Captive balloon	CB1	CUF	Nuevos Ministerios	40° 26′ 45.6″	3° 41′ 27.6″	686
Meteorological network	MN1	CUF	CIEMAT	40° 27′	3° 43′	680
	MN2	OUA	Fuencarral	40° 30′ 06″	3° 40′ 57″	729
	MN3	–	Junta Mpal. Moratalaz	40° 21′ 34″	3° 34′ 10″	687
	MN4	DUF	Junta Mpal. Villaverde	40° 20′ 58″	3° 42′ 39″	594
	MN5	–	E.D.A.R. La China	40° 19′ 26″	3° 40′ 42″	566
	MN6	DUF	Centro Mpal. De Acústica	40° 26′ 43″	3° 44′ 24″	587
	MN7	DUF	Junta Mpal. Hortaleza	40° 27′ 49″	3° 39′ 24″	704
Surveillance network	SN1	CUF	Pza. de España	40° 25′ 26.94″	3° 42′ 43.52″	637
	SN2	DUF	Pza. de Castilla	40° 28′ 05.77″	3° 41′ 19.14″	729
	SN3	–	Casa de Campo	40° 25′ 12.35″	3° 44′ 57.22″	645
AEMET stations	AS1	CUF	Madrid-Parque Retiro	40° 24′ 40″	3° 40′ 41″	667
	AS2	OUA	Madrid Barajas	40° 27′ 15″	3° 32′ 39″	582
	AS3	DUF	Madrid-Cuatro vientos	40° 22′ 40″	3° 47′ 21″	687
	AS4	OUA	Madrid Getafe	40° 18′ 00″	3° 43′ 21″	617
	AS5	DUF	Madrid-Ciudad Universitaria	40° 27′ 10″	3° 43′ 27″	664
	AS6	OUA	Madrid Torrejón de Ardoz	40° 29′ 00″	3° 27′ 01″	611
	AS7	OUA	Colmenar Viejo	40° 41′ 55″	3° 45′ 52″	1004
Fixed masts	FM1	DUF	Rugby field UAM	40° 32′ 50.58″	3° 41′ 53.57″	–
	FM2	DUF	Firemen Park tower	40° 23′ 39.98″	3° 39′ 13.11″	–
	FM3	CUF	New city Hall	40° 25′ 8.35″	3° 41′ 31.88″	–
	FM4	CUF	Printing	40° 24′ 49.96″	3° 42′ 19.87″	–
	FM5	DUF	Urbanism building	40° 27′ 36.31″	3° 40′ 19.86″	–

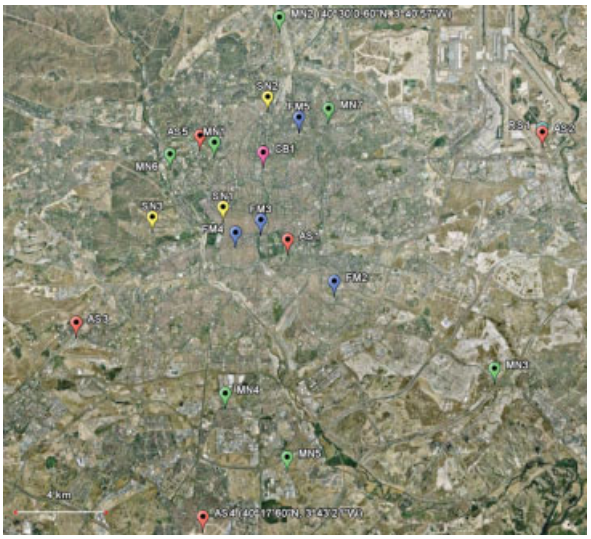

Figure 2. Location of the atmospheric measurements sites in DESIREX campaign. See Table I for icons identification. The Earth Coordinates for the MN2 and AS4 sites are indicated. (Picture obtained from Google Earth).

light winds during the two days studied. This kind of synoptic situation favours, in rural areas during the night, the development of surface-based thermal inversions, with strong stability; in these situations, the topographic features cause the development of circulations that are far from being non-divergent over Madrid, and convergence katabatic flows can reach the city (Terradellas and Cano, 2007).

The 60-h simulations begin at 1800 UTC (LST = UTC + 2 h) 29 June and finish at 0600 UTC 2 July. The first 6 h are not considered for the analysis of the results; only the following 48 h (two days) are taken into account. The horizontal domain of the simulations was composed of five two-way nested domains with 100×100, 174×156, 219×186, 216×198, and 240×270 grid points, and a grid spacing of 27, 9, 3, 1, and 0.333 km, respectively. The 60-h simulations were conducted with the initial and boundary conditions obtained from the operational National Centre for Environmental Prediction (NCEP) with a grid resolution of 40 km and a time resolution of 3 h. To take full advantage of the urban parameterisations, a vertical resolution of *51* eta levels (Full eta levels = 1., 0.998743415, 0.99748677, 0.996230185, 0.9949736, 0.993716955, 0.992334723, 0.990814209, 0.989141703, 0.987301886, 0.98527813, 0.983051956, 0.980603218, 0.977909565, 0.974946558, 0.971687257, 0.968101978, 0.964158237, 0.959820092, 0.955048144, 0.949799001, 0.94402492, 0.937673509, 0.930686891, 0.923001587, 0.914547801, 0.905248582, 0.895019472, 0.883767486, 0.871390283, 0.857775331, 0.842798889, 0.826324821, 0.80820334, 0.788269699, 0.7663427, 0.742223024, 0.715691328, 0.68650645, 0.65440315, 0.619089544, 0.580244482, 0.537514985, 0.49051252, 0.438809812, 0.381936818, 0.319376528, 0.250560224, 0.17486228, 0.0915945247, and 0.0000. The vertical coordinate eta is defined as $(p - p_{top})/(p_{surf} - p_{top})$, where p is the dry hydrostatic pressure at each corresponding level, p_{surf} is dry hydrostatic surface pressure, and p_{top} is a constant dry hydrostatic pressure at model top.) was used (33 levels in the lowest 1.5 km with the domain top over ≈20 km). The selected radiation parameterisations were the Dudhia (1989) shortwave radiation scheme, and the Rapid Radiative Transfer Model (RRTM) longwave parameterisation (Mlawer *et al*., 1997). The microphysics package was WSM3 (Hong *et al*., 2004); no cumulus cloud scheme was used in the inner domain.

Four different simulations with the BEP+BEM scheme (Table II) were performed using the non-hydrostatic version V3.2 of WRF (Skamarock *et al*., 2008), coupled to the Noah land surface model (LSM, Chen and Dudhia, 2001) for the vegetated part. Two simulations were run with the one-and-a-half-order closure Bougeault and Lacarrère (1989) turbulent scheme (BL, hereafter they

Table II. Summary of the different simulation scenarios.

Simulation Scenarios	pbl2(AH)	pbl8(AH)	kh_pbl2(AH)	kh_pbl8(AH)
Horiz. Diff. Treatment	Smagorinsky first order	Smagorinsky first order	Constant value	Constant value
PBL scheme	MYJ	BL	MYJ	BL
AH	Yes	Yes	Yes	Yes
Ejected				
Albedo increased	No	No	No	No
Insulating material	No	No	No	No
Simulation Scenarios	kh_pbl8(noAH)	kh_pbl8(AH)_ALB	kh_pbl8(AH)_INSULATION	kh_pbl8(noAH)_ALB_INSULATION
Horiz. Diff. Treatment	Constant value	Constant value	Constant value	Constant value
PBL scheme	BL	BL	BL	BL
AH	No	Yes	Yes	No
Ejected				
Albedo increased	No	Yes	No	Yes
Insulating material	No	No	Yes	Yes

are referred as pbl8(AH), and kh_pbl8(AH) respectively), and the other two with the two-order closure Mellor-Yamada-Janjic (Janjic, 1994) turbulent scheme (MYJ, cases pbl2(AH), and kh_pbl2(AH), respectively). The BEP+BEM parameterisation only can be run with these two turbulent schemes in the WRF model so far. For pbl2(AH) and pbl8(AH), the Smagorinsky first-order closure scheme (default option in WRF) is used in the horizontal. However, these simulations, during daytime, generated some spurious rolls-type structures within the central part of the domain. It is debatable whether these structures have a counterpart in the real world or they are a numerical artefact of the model. Unfortunately, there are no measurements available to decide this. To get indirect information on this matter, in the two kh_pbl8(AH) and kh_pbl2(AH) runs, the horizontal diffusion coefficient (kh) was fixed to 300 m^2s^{-1} to filter the roll-types structures. Different studies, for example Lemone *et al.* (2010) have used this constant value for the horizontal diffusion coefficient (personal communication) showing good performances when high-resolution (sub-km) runs were carried out with WRF. The comparison against point measurements and vertical soundings could help to identify the best approach.

WRF runs coupled to the Noah land surface model (Chen and Dudhia, 2001) for the vegetated part, which has one canopy layer and the following prognostic variables: soil moisture and temperature in the soil layers, water stored in the vegetation canopy, and snow stored on the ground.

BEP+BEM scheme is a building energy model linked to a multilayer UCP (BEP, Martilli *et al.*, 2002) that takes into account the exchange of energy between the buildings and the outdoor atmosphere. BEP takes into account the effects of the building vertical and horizontal surfaces on momentum (drag force approach), turbulent kinetic energy, and potential temperature. The radiation at walls and roads considers shadowing, reflections, and trapping of shortwave and longwave radiation in street canyons. In BEM, the evolution of the indoor air temperature is computed as a function of the energy production and consumption in the buildings (separately for every floor) as well as the impact of the AC system. Obviously, the indoor surface temperature is not fixed constant during the simulation, but an energy budget is solved in each indoor surface. In this way, the evolution of the meteorological variables is practically independent of the initial wall temperatures. The AH released into the urban atmosphere to maintain the indoor air temperature in a comfort range, is computed through an AC model (more details in Salamanca *et al.*, 2010a). Assuming that the AC systems were working in the studied period (hot summer days), the AH was ejected into the atmosphere in the four mentioned simulations.

Three different urban classes were defined in the inner domain (Figure 3) based on the CORINE (Coordination of Information on the Environment) land cover (the inventory was of the year 2000) database from the European Environment Agency (http://www.eea.europa.eu): 'continuous urban fabric' (CUF), 'discontinuous urban fabric' (DUF), and 'other urban areas' (OUA) that represents a collection of points that in the CORINE database were classified as 'Industrial or commercial units', 'Road and rail networks and associated land', and 'Airports'. The CUF class covered a surface of 102.42 km^2, the DUF class of 423.67 km^2, and finally the OUA class of 177.89 km^2. For the non-urban part (Figure 3), an up-to-date MODIS-based land use classification was used.

The urban parameters and thermal properties defined for every urban class can be seen in Tables III and IV, respectively. The thermal properties for the roofs and walls represent surfaces built with bricks and concrete, which are common construction materials in Madrid. In the case of roads, the default values in WRF were

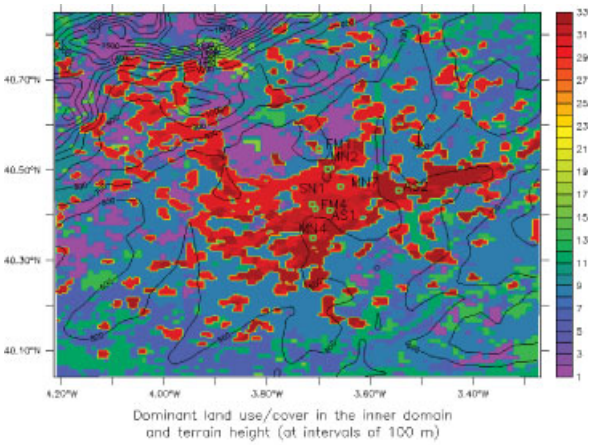

Figure 3. Up-to-date MODIS-based land use classification (20 + 3 urban categories) used in the inner domain. In the figure, the 31, 32, and 33 (DUF, CUF, and OUA) values correspond to points where the urban fraction is more than 0. Continuous black lines correspond to height a.s.l. (The Central System Mountains at the NW of the domain can be seen). The location of the AS2, AS1, FM1, FM4, MN2, MN4, MN7, and SN1 measurements sites is indicated with green square marks.

Table III. Urban morphological parameters considered for the three urban classes.

Parameter	CUF (High Intensity Residential)	DUF (Low Intensity Residential)	OUA (Commercial or Industrial)
Building plan area fraction	0.60	0.50	0.375
% of buildings of 5 *m* of height	5	15	10
% of buildings of 10 *m* of height	15	55	20
% of buildings of 15 *m* of height	15	25	40
% of buildings of 20 *m* of height	65	5	30

Table IV. Thermal parameters used in the urban module BEP+BEM for the three urban classes.

Surface	$\lambda(Wm^{-1}\ K^{-1})$	$C(\cdot 10^6\ Jm^{-3}\ K^{-1})$	ε	α	$z_0(m)$
Roof	0.695	1.32	0.9	0.2	0.01
Wall	0.695	1.32	0.9	0.2	–
Road	0.4004	1.40	0.95	0.15	0.01

λ is the thermal conductivity of the material, C is the specific heat of the material, ε is the emissivity of the surface, α is the albedo of the surface, and z_0 is the roughness length for momentum over the surface.

considered reasonable. For the correct performance of the BEP+BEM scheme (Salamanca *et al.*, 2010a) extra inputs are required, and the values used were similar the ones considered for the city of Basel (Salamanca and Martilli, 2010). In the three urban classes, the coverage area fraction of windows in the walls was fixed to 0.2, the number of occupants to 0.02 person/m^2 of floor, and a thermal efficiency of the total heat exchanger to 0.75 (this value means the indoor air of buildings is replaced by fresh air six times a day that corresponds to normal conditions). For the AC model, additional parameters are needed and were fixed to the following values: target internal temperature 25 °C, amplitude of range of comfort 1 °C, and COP (Coefficient of Performance of the AC systems) 3.5 (standard value). The peak heat flux generated by equipments was 36 Wm^{-2} of floor for OUA areas, and 20 Wm^{-2} for the rest of urban classes. The considered values for the sensible heat generated by equipments are similar to others estimations based on temporal variations of electric power consumption (Kikegawa *et al.*, 2003).

3.2. Analysis of the results

3.2.1. Air temperature

The meteorological air temperature sensors were displayed at different heights, often above roof level, depending on the location and type of station. For this reason, the measurements instead of being compared with the standard modelled 2 m-air temperature were compared with the second eta level above ground (≈10 m) that was more representative (the height of the lowest mesoscale model level was about ≈5 m). The Root Mean Square Error (RMSE) and Mean Bias (MB, obs.-simulated) results for the air temperature can be seen in Figures 4–7 for the four (AH) simulations.

Observing Figures 4(a)–7(a), an important difference can be pointed out; the simulations with the BL turbulent scheme produced the best results. On the other hand, when the horizontal diffusion coefficient was fixed, the RMSEs were reduced independently of the turbulent scheme (BL or MYJ) considered. *A priori*, there is no reason to justify the best performance of the BL turbulent scheme. Both turbulent schemes solve a prognostic equation for the TKE, and the differences are in the way the length scales and turbulent coefficients are estimated. For the four simulations, the MB was almost positive for all the stations, indicating that the model (in average) slightly underestimates the air temperature. A reason for this can be that other anthropogenic heat sources are still missing in the model (e.g. traffic).

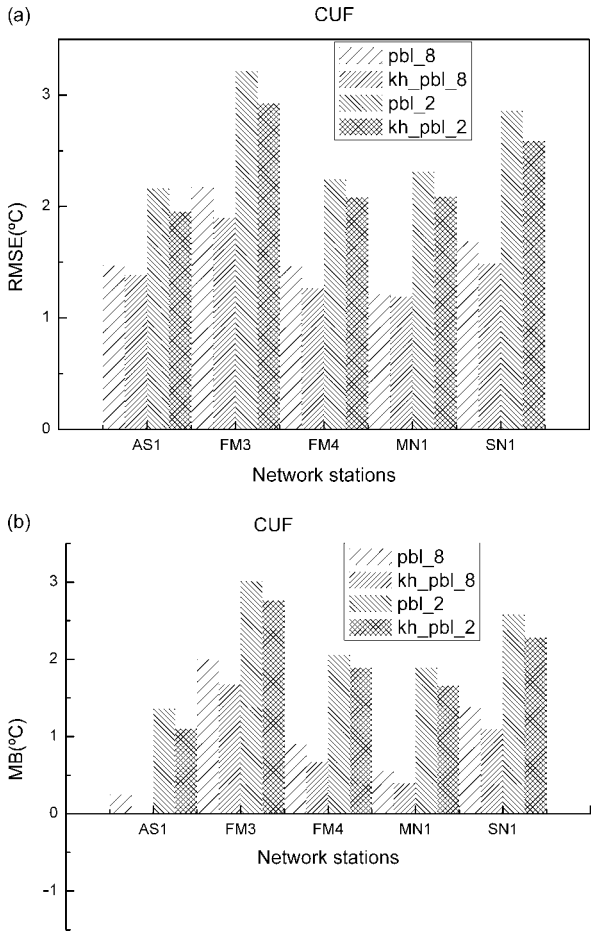

Figure 4. Statistical parameters for the air temperature computed in the CUF stations: (a) RMSE, and (b) MB.

Analysing in more detail the kh_pbl8(AH) (as the run that produces the best results) simulation and taking into account the urban classification, we can say that for the majority of the stations the RMSEs are below 1.5 °C in the CUF and OUA areas, and above 1.5 °C in the DUF and RURAL areas. This fact could mean that the densest urban and commercial zones are better represented with the urban parameters of Table III than the low residential areas.

To study the effect of the AC systems on the air temperature, the RMSE (no AH) and MB (no AH) have been computed for a new run (hereafter it is referred as kh_pbl8(noAH), see Table II) for which the AH fluxes

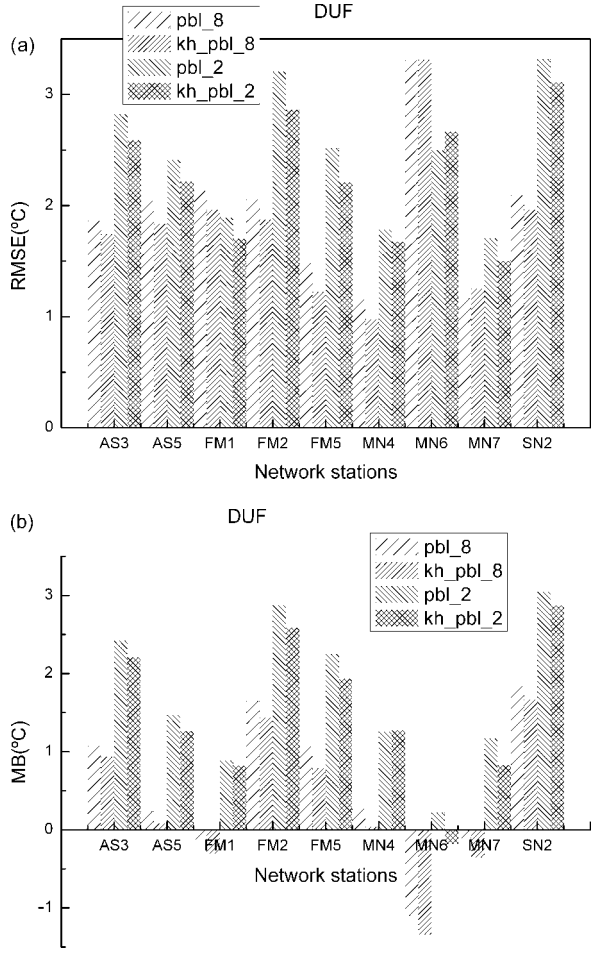

Figure 5. As in Figure 4, but at DUF stations.

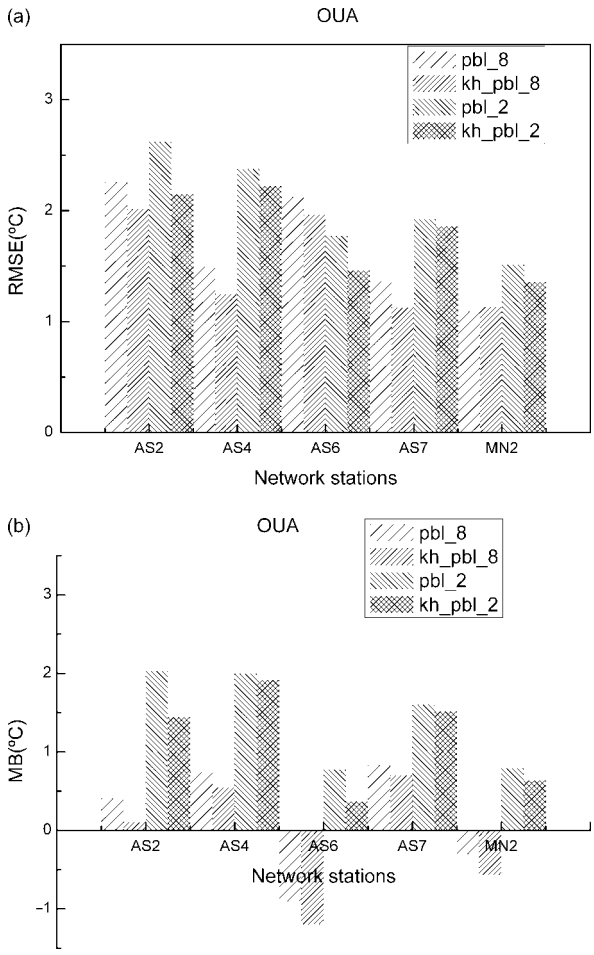

Figure 6. As in Figure 4, but at OUA stations.

coming from the AC systems were removed. The best results obtained with the kh_pbl8 run were sufficient reason for conducting the sensitivity analysis with this particular setup. Comparing the statistical parameters of both simulations kh_pbl8(AH) and kh_pbl8(noAH), the effect of the AH has been analysed. The results are summarized in the Figure 8(a) and (b) for all the stations. Figure 8(a) shows that the RMSE improved (in most of the stations) when the AH was considered, as the MB (Figure 8(b)). The effect of the AH is not constant during all the day (not shown), but it is linked to the urban fraction of the corresponding area. Figure 9 shows the 2-m air temperature differences obtained with the two kh_pbl8 simulations (T2(AH)-T2(no AH)) at 1800 UTC (when this difference is maximum during daytime) for 30 June together with boundary line of urban fraction in the inner domain. Clearly, both patterns overlap, and differences up to 1.5 °C are reached in the urban core showing the significant effect of the AH especially in those zones where the urban factor is predominant. The AH can affect the intensity of the UHI and the vertical structure of the atmosphere as we will see in Section 4.

Taking into account the total number of stations and the statistical values obtained, we can claim that the inclusion of the AH in the BEP+BEM scheme, improved the results in most of the stations spread out over the city and surroundings, although we are aware that an exact quantification of the AH and its effect would require more information that was not available for Madrid (high-resolution urban morphology, correct target temperature, percentage of buildings with air conditioning systems, etc.)

3.2.2. *Wind surface measurements*

One of the most important problems in the comparison between wind measurements and mesoscale model results in urban areas is the possible impact in the measurement of microscale effects not captured by the model's resolution. The impact of these microscale effects on the air temperature is less important than on the wind field. For example, the wind field inside an urban canyon not aligned with the direction of the predominant mesoscale wind field could be totally different due to the presence of buildings. For this reason, in urban areas, the position of a meteorological station plays a fundamental role. The position of the station must be sufficiently distant from walls and roofs to avoid these local effects. Detailed information on the exact position of the stations in the microscale structure of the city is not available, but it is likely that the position can explain part of the differences between model results and measurements.

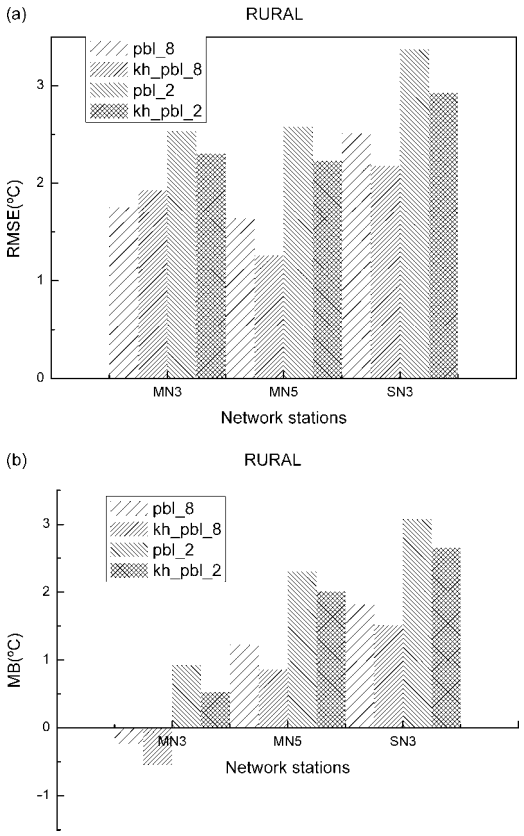

Figure 7. As in Figure 4, but at RURAL stations.

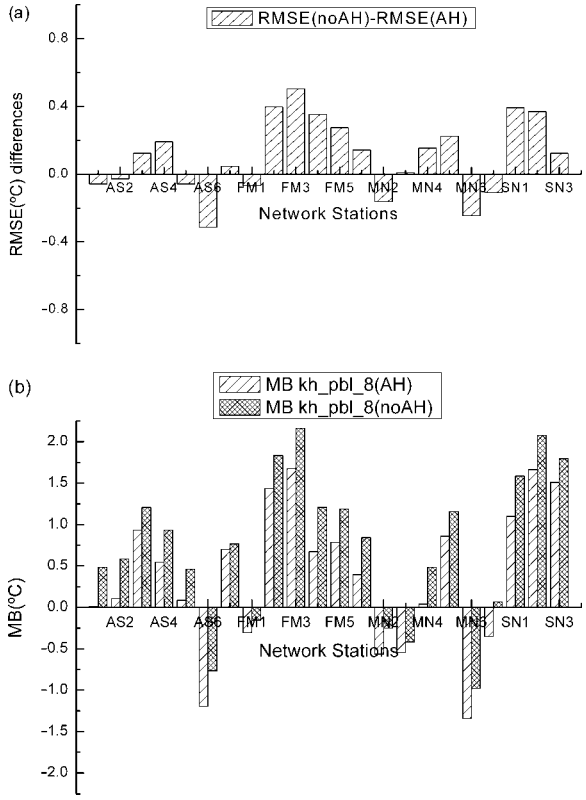

Figure 8. Statistical parameters computed for the two kh_pbl8(AH) and kh_pbl8(no AH) simulations: (a) RMSE (no AH)-RMSE(AH), and (b) MB for both simulations.

The comparisons have shown that the simulations obtain the best results with the horizontal diffusion at 300 m^2s^{-1}. For this reason only these simulations (kh_pbl8(AH) and kh_pbl2(AH)) are analysed here. The wind speed (at 10 m agl) for the kh_pbl2(AH) and kh_pbl8(AH) is compared against observations in three different sites, MN4, AS1 and MN7 (Figure 10(a)–(c). The MN4 site is an urban area situated at the south of the city, while the MN7 is an urban site surrounded by green areas situated in the northeast part of the city. The AS1 site represents an urban park (Retiro) close to the city centre. The model captured reasonably well the wind speed and wind direction the first day of simulation, but not the second day (1 July) where the model has some problems to capture correctly the wind direction (lower parts of the Figure 10(b) and (c). Although some discrepancies can appear at some hours, the differences observed between the two simulations were not significant. A similar behaviour has been observed for other stations (not shown). Recent studies (Hu *et al*., 2010) have demonstrated that the choice of the PBL scheme in WRF can affect the wind speed profiles, however in this work, the wind speed only has been evaluated at 10 m agl and not important differences have been observed between the two turbulent models. A detailed study of the sensitivity of the results to others PBL schemes, initial soil conditions, and boundary conditions could help to understand the origin of the disagreement between model results and measurements for the second day of simulation. However, as mentioned above, it goes beyond the scope of this article.

In order to evaluate the impact of the anthropogenic heat, we have commented that another simulation was done without ejecting the AH into the atmosphere (kh_pbl8 (noAH). In Figures 11–13 temporal evolutions of the measured wind speed against modelled (at 10 m agl) are displayed in the sites mentioned above for the two kh_pbl8 (AH and no AH) runs. There are no important differences between the two kh_pbl8(AH) and kh_pbl8(no AH) runs, showing that the AH does not affect significantly the wind speed close to the ground. It is important to comment that the AC system adopted in BEP+BEM is a 'vertical-wall' system, and consequently, the AH generated in each floor is ejected at the corresponding vertical layer. This adopted system is more appropriate than a 'roof-top' system for mesoscale simulations as is indicated in Sailor (2011).

4. UHI and evaluation of energy consumption mitigation strategies

4.1. Urban *Heat Island*

The UHI is a known phenomenon very common in urban environments. The trapping of radiation that takes place in the urban canopy, the thermal properties of the building materials, and the AH due to human activities are the principal factors that generate the UHI. The UHI during heatwave episodes can represent a significant risk for the

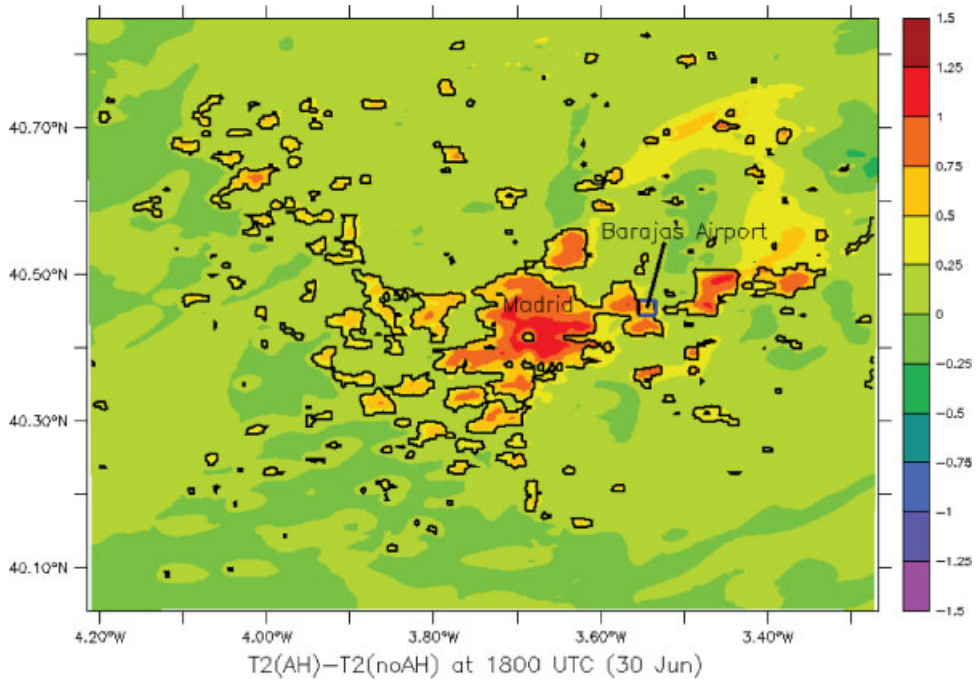

Figure 9. T2(AH)-T2(no AH) differences obtained with the two kh_pbl8 simulations at 1800 UTC for 30 June together with boundary line of the urban fraction. Barajas Airport location is indicated with a square mark.

population. A recent review on urban climate, including turbulence, exchanges of energy and water, and the urban heat island can be found in Arnfield (2003).

In this section, the urban heat island of Madrid has been analysed by means of the kh_pbl8(AH) simulation, since it is the best run compared to measurements. In Figure 14(a), the 2-m air temperature (kh_pbl8(AH) case) at 2200 UTC (30 June) has been plotted. Clearly, the UHI is completely developed during the nocturnal time, and covers the totality of the urban areas with different degrees of intensity. Areas with greater building plan area fraction present a higher UHI intensity (compare Figure 14(a) with Figure 3) and areas with low urban fraction and lower intensity. It is interesting to observe that the increase of temperature at night reaches even areas that are fairly distant from the city due to the advection of the accumulated heat. The UHI intensity is spatially dependent within the urban area, and it can be observed in the figure that the magnitude could reach up to 5–6 °C, which is in agreement with the values found by Yagüe *et al*., (1991). It is interesting to observe the effect of the AH in the magnitude and extension of the UHI. For this reason (Figure 14(b)), the 2-m air temperature difference at 2200 UTC (30 June) has been plotted for the kh_pbl8(AH) and kh_pbl8(no AH) runs. Differences of 1.25–1.5 °C can bee seen over the city, even greater than 2 °C in the eastern part, showing clearly the effect of the AH in the intensity of the UHI.

One of the important consequences of the larger nocturnal heating in the city compared to the urban surroundings is the weaker surface-based thermal inversions formed (clearly seen in Figure 15(a)) due to the warmer core of the city. It is important to mention that the inner domain presents strong variations in height and, consequently, the UHI intensity could be misinterpreted. For this reason, a vertical ZY section of potential temperature (longitude = 3.70 W) is plotted in Figure 15(a) and (b). The air temperature difference between central areas of the city (≈latitude = 40.4 N) and southern (≈latitude = 40.15 N) areas (points with the same height asl) reached up to 5 °C (Figure 15(a)). Observing the two Figure 15(a) and (b), we can see as the AH affects not only the UHI intensity, but also the vertical structure of the atmosphere in the first hundreds of meters. Thanks to the consideration of the AH fluxes, the model was able to reproduce a nocturnal mixing layer over the city with a thickness of approximately 200 m.

Finally, the temporal evolution of 2-m air temperature differences between couples of rural–urban stations has been analysed (kh_pbl8(AH)). In Figure 16(a), results for the SN1 (into the city centre) and AS2 (outside the city) stations are shown. Owing to the small differences in height (Table I), the magnitude of the plots represents the real intensity of the UHI. Although the model is not able to reproduce the maximum magnitude of the UHI, it is able to capture reasonably well the tendency of the curve. Differences between the couple FM4 and MN2 are plotted in Figure 16(b). Owing to differences in height, this picture does not represent the real magnitude of the UHI, but the influence of the urban core is clear. In this case, the model was able to capture the maximum magnitude of the air temperature differences, even if with a slight time delay.

Summarising, the Madrid metropolitan area experiments strong nocturnal UHI in summer periods with intensities that can reach up to 5–6 °C in some regions of the urban area.

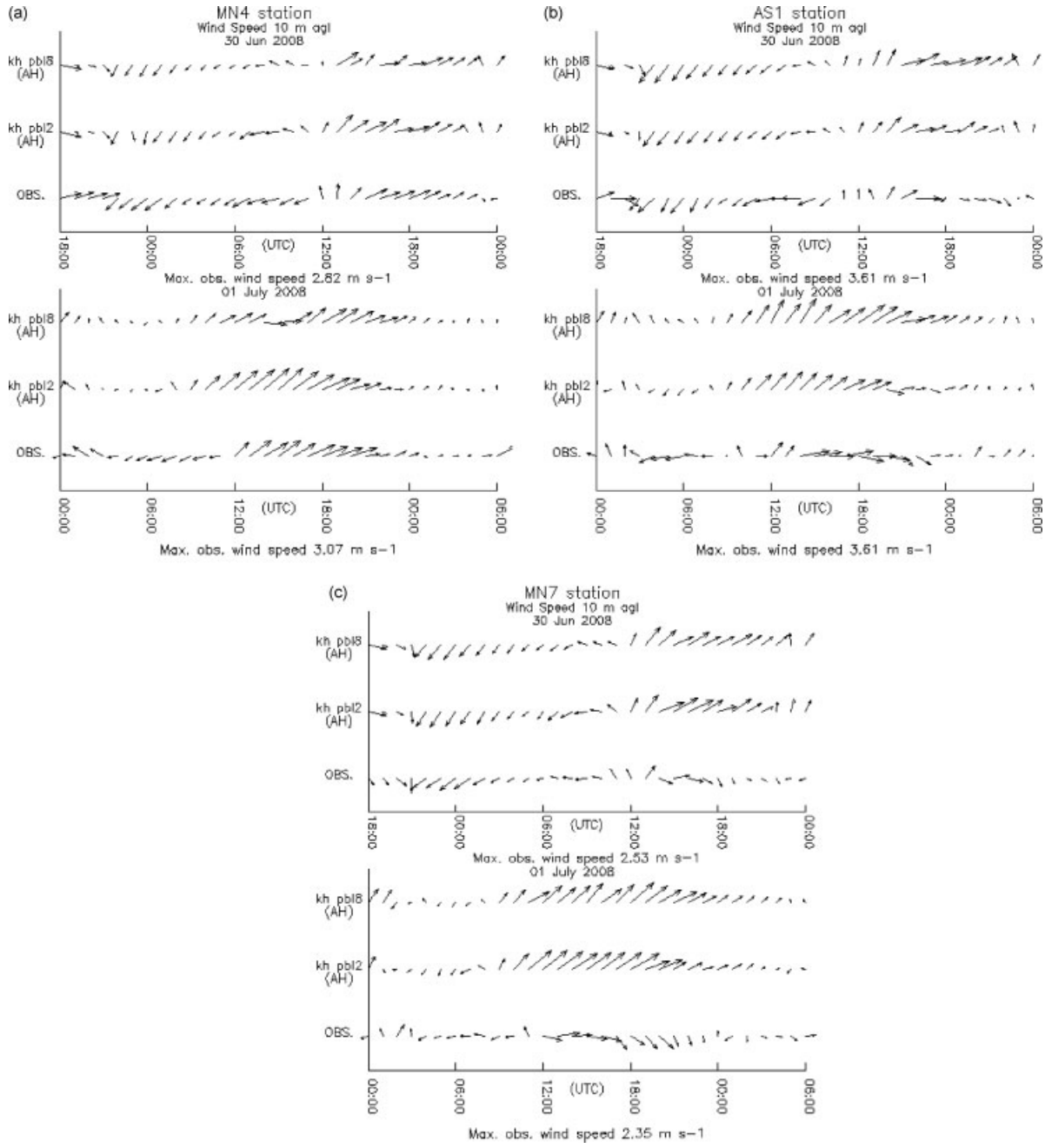

Figure 10. Temporal evolutions of the horizontal wind speed at 10 m agl obtained with the kh_pbl2(AH) and kh_pbl8(AH) runs against observations: (a) 30 Jun (upper plot) and 1 July (lower plot) at MN4 site, (b) 30 Jun and 1 July at AS1 site, and (c) 30 Jun and 1 July at MN7 site.

4.2. Energy consumption mitigation strategies

In the last few years, different strategies have been proposed to mitigate the UHI in several cities around the world. With the double objective of improving the urban climate and reducing the related energy consumption (AC systems), the principal strategies to reduce UHI intensity and energy consumption in urban areas are high albedo surfaces, urban forestry (planting trees in open spaces), green roofs, and new building materials with different thermal properties (Rosenzweig *et al*., 2009), although some of them could have negative effects on air quality (e.g. reducing the mixing height). In BEP+BEM the energy consumption due to AC systems can be computed and different strategies can be evaluated. In this section, three strategies are analysed (by means of three kh_pbl8 new simulations, in Table II) without considering the possible impacts on air quality: the first consists in a change of the albedo of the roofs from 0.2 to 0.4 (hereafter referred as kh_pbl8(AH)_ALB case), the second, consists in a modification of the thermal properties of the roofs (Table IV) by introducing an internal layer of 6 cm of insulating material (specific heat $C = 0.382$ M Jm^{-3} K^{-1}, and thermal conductivity $\lambda = 0.09$ W m^{-1} K^{-1}) (kh_pbl8(AH)_INSULATION

Table V. Saving energetic produced in every urban class and over the Madrid metropolitan area.

STRATEGIES	% OUA	% CUF	% DUF	% TOTAL
kh_pbl8(AH)_ALB	3.61	4.42	5.56	4.82
kh_pbl8(AH)_INSULATION	2.41	3.00	4.39	3.59
kh_pbl8(noAH)	2.11	3.59	2.33	2.54
Kh_pbl8(noAH)_ALB_INSULATION	7.26	10.02	11.12	9.90

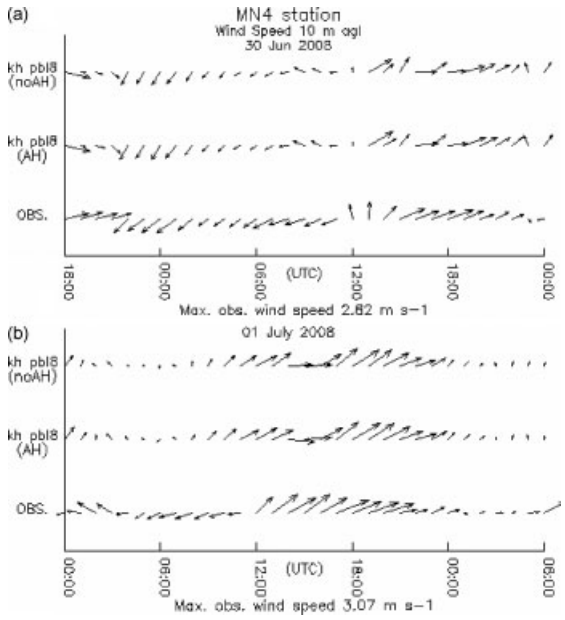

Figure 11. Temporal evolutions of the horizontal wind speed (at 10 m agl) at MN4 site with the kh_pbl8(no AH) and kh_pbl8(AH) runs against observations: (a) 30 Jun, and (b) 1 July.

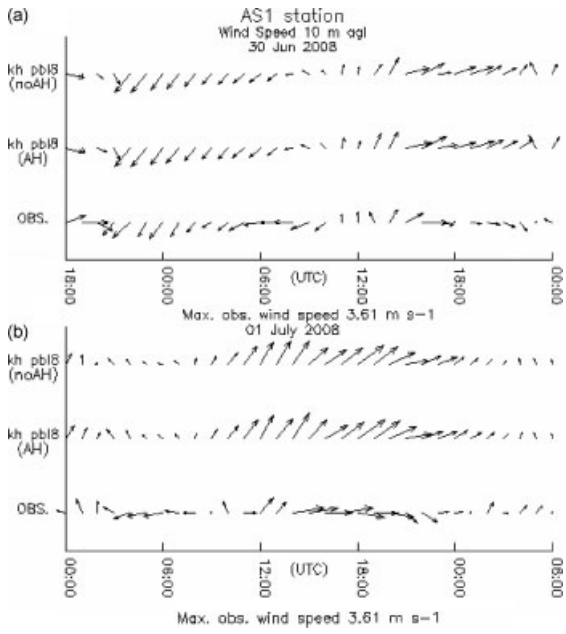

Figure 12. As in Figure 11, but at AS1 site.

case), and finally the third (kh_pbl8(noAH)_ALB_INSULATION case) groups the mentioned modifications (change in the albedo, introduction of the insulating material, and no ejection of the AH into the atmosphere) into a single strategy. To evaluate the impact on the UHI, the 2-m air temperature has been analysed at 2200 UTC (30 June) for the three cases. Comparing the kh_pbl8(AH)_ALB case against the previous kh_pbl8(AH) simulation, it can be seen that areas with greater temperatures (29–30 °C) have been reduced, and the total daily energy consumption (EC) was decreased by 4.82% (Table V). The total EC when the AH is not ejected into the atmosphere (kh_pbl8(noAH) simulation) was reduced by 2.54%, showing the existing feedbacks between the AC systems and the outdoor temperature. From the point of view of energy saving, the albedo strategy was better than the no AH strategy. Although the increase of the albedo is a known approach to reduce the UHI and EC in summer conditions, it could be counterproductive for winter periods (an increase in winter heating energy consumption was found by Saiz *et al*., 2006). No appreciable differences appear when the two cases kh_pbl8(AH) and kh_pbl8(AH)_INSULATION are compared. It seems that the insertion of insulating material would affect the total EC (the total consumption was reduced in a 3.59%) but not the nocturnal UHI because the heat released through the exterior walls during the night would be similar in both simulations. An important energy saving was obtained

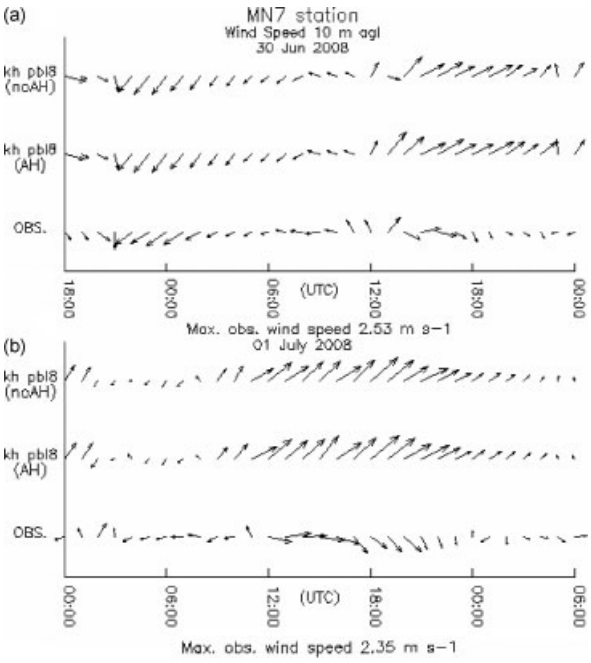

Figure 13. As in Figure 11, but at MN7 site.

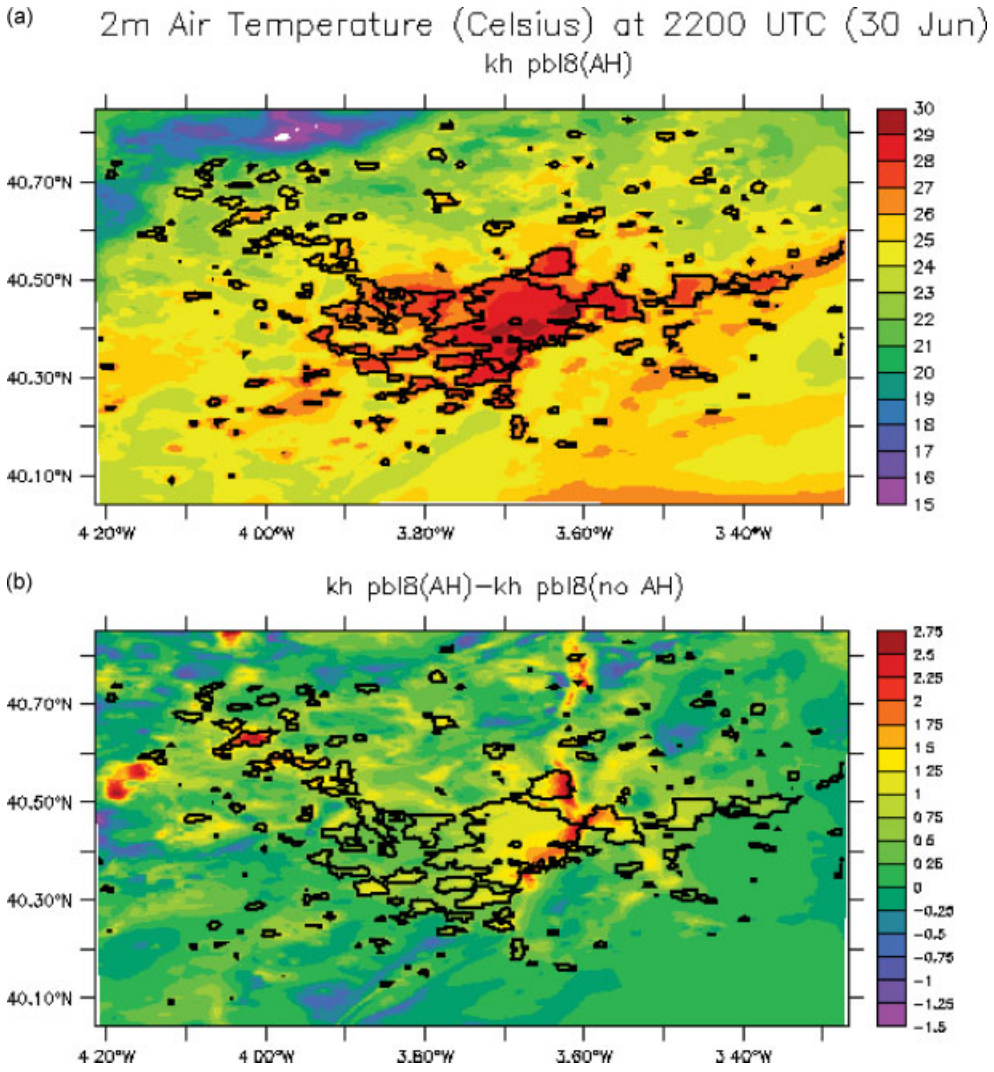

Figure 14. 2-m air temperature (°C) at 2200 UTC (30 Jun); (a) kh_pbl8(AH) run, and (b) difference kh_pbl8(AH)-kh_pbl8(no AH).

with the kh_pbl8(noAH)_ALB_INSULATION strategy reaching up to 9.90%. It is interesting to mention that the sum of the energy saving obtained with every strategy separately (change in the albedo of the roofs, introduction of the insulating material, and no ejection of the AH into the atmosphere) is bigger than the energy saving obtained with the kh_pbl8(noAH)_ALB_INSULATION simulation. This fact is explained because the air temperature, the EC, and the ejected AH are physical magnitudes interconnected and strongly dependent. A considerable reduction of the UHI (1–2 °C) was observed in some urban areas when the two cases kh_pbl8 against kh_pbl8(noAH)_ALB_INSULATION are compared. Finally, in the Table V, results of the energy saving obtained with every strategy and for every urban classes (classification derived from the CORINE database) are shown. The greatest saving for the kh_pbl8(noAH) strategy took place in the CUF areas that curiously represent the smallest coverage extension. In these areas, the urban fraction is practically 100%, and the building plan area fraction represents 60% (Table III). These morphological parameters increase the AH emissions (in some way the AH released by the AC systems is 'proportional' to the total volume of air trapped inside the buildings), and consequently the energy saving was greater in these areas. On the other hand, observing the other strategies analysed, the greatest saving coincided with the more extensive areas (DUF). It is not possible to generalize the conclusions because the results can be strongly linked to urban morphological parameters (Table III) that could be different for other cities.

5. Conclusions and future work

In this paper, a new UCP (BEP+BEM) has been tested over the Madrid metropolitan area with the WRF model in summer conditions. The urban scheme is integrated in the public release WRF V3.2 since April 2010. This UCP represents the most sophisticated urban parameterisation coupled to the WRF model to date, and it considers the heat (sensible/latent) fluxes exchanged between the buildings and the atmosphere. Two consecutive days (with synoptic conditions that favoured the formation

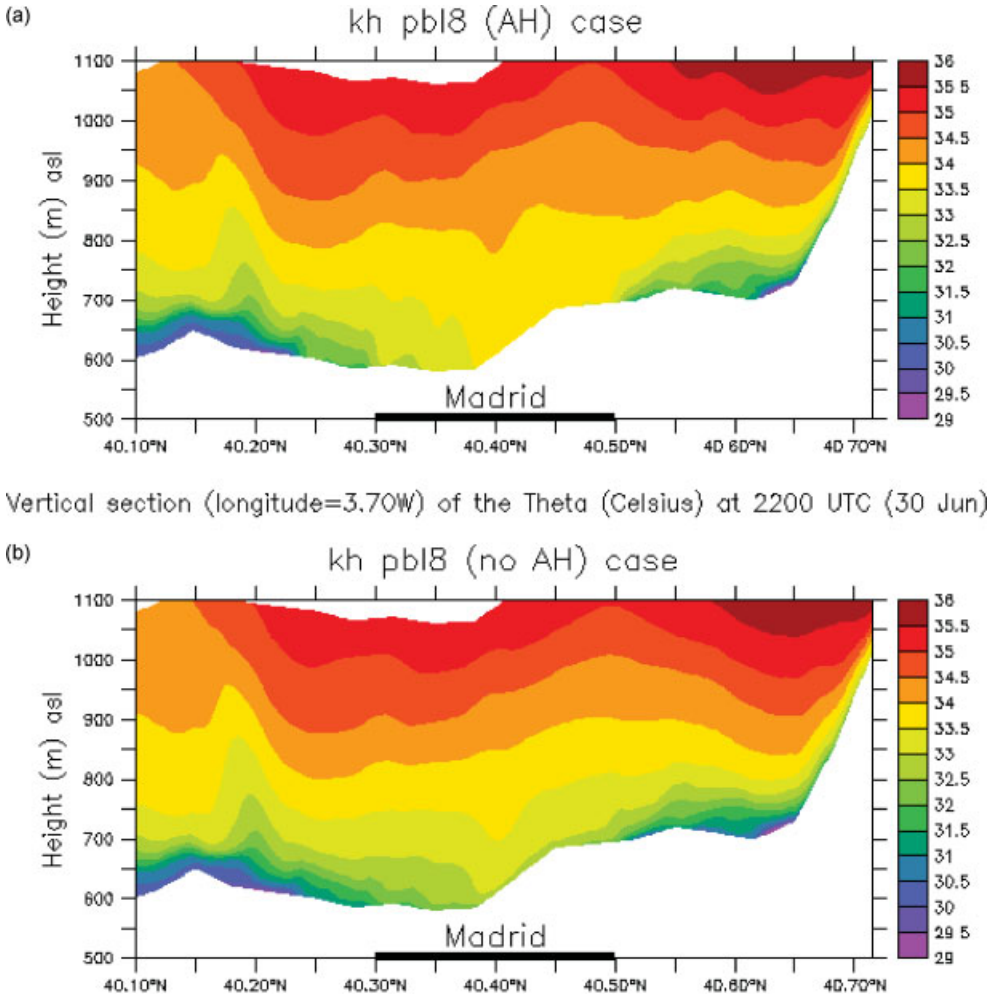

Figure 15. Vertical section (longitude = 3.70 W) of the air potential temperature θ(°C) at 2200 UTC (30 June) over the city of Madrid; (a) kh_pbl8(AH) case, and (b) kh_pbl8(no AH) case.

of the UHI) have been analysed (30 June and 1 July) and model results have been compared against measurements recorded in the DESIREX 2008 campaign. The urban model was able to reproduce satisfactorily the air temperature over the period analysed especially when the horizontal diffusion coefficient was fixed to 300 $m^2\ s^{-1}$ together with the Bougeault and Lacarrère turbulent scheme. On the other hand, the wind field over the city is more difficult to validate and is strongly dependent of the mesoscale circulations in the surroundings areas. In any case, the wind field was captured reasonably well the first day of simulation, and some difficulties appeared the second day for all the cases. It would be interesting to extract more definitive conclusions analysing the results for a longer time period, but this is left for a future work. The impact of the AH due to space cooling loads (peaks up to 110 W m^{-2} were reached in the middle of the afternoon) and their EC was evaluated and different mitigation strategies were addressed. At some daytime hours, AH was responsible of an increase in the air temperature up to 1.5 °C.

The UHI over Madrid reached up to 5–6 °C in some urban regions. The total EC was reduced by 4.8% when the roof albedo was increased and by 3.6% when an insulating material was introduced in the roofs. A high albedo at the roofs, the use of insulating materials inside the walls, and AC systems that do not directly eject heat into the atmosphere are different strategies that could significantly reduce the UHI (1–2 °C) and EC (an energy saving up to 10% was obtained).

It is important to mention here that to quantify correctly the AH released in an urban area through an UCP, detailed information of the urban morphology is necessary, and high-resolution urban canopy parameters datasets are recommended. The spatial and temporal variations of the AH, UHI, and EC over a city are physical magnitudes difficult to quantify without a detailed up-to-date urban morphology data. In this case, a detailed land use based on CORINE is used, but little information is available on urban morphology (building height, street width, etc.). The results shown, then, mainly give an idea of the potentiality of the approach, and the order of magnitude that can be expected in particular for the energy consumption.

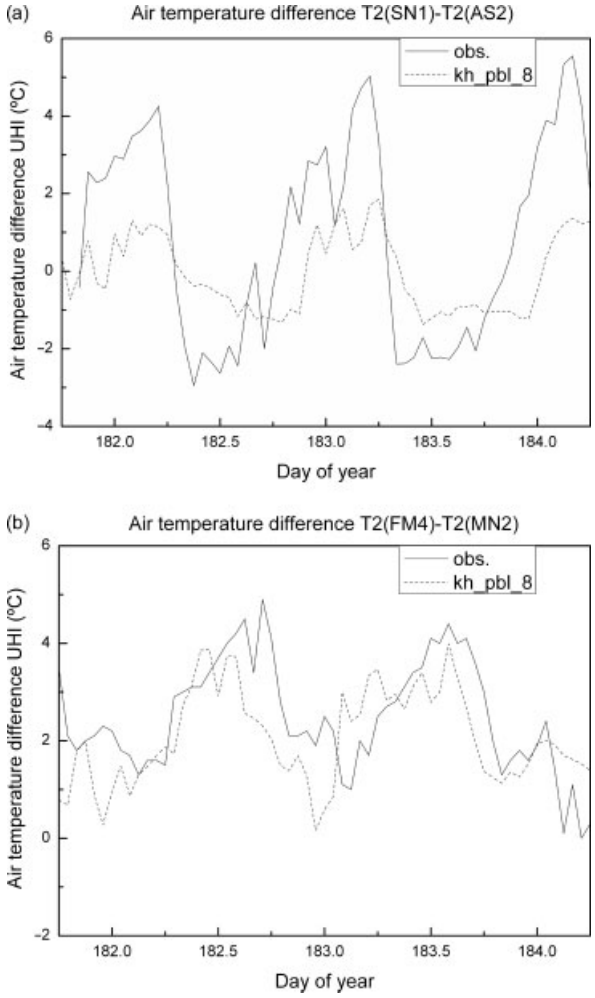

Figure 16. Temporal evolution differences of the 2-m air temperature between two sites showing the evolution of the UHI (measured against modelled, kh_pbl8(AH)): (a) SN1 and AS2 sites, and (b) FM4 and MN2 sites.

Acknowledgements

We thank CIEMAT for the doctoral fellowships held by Francisco Salamanca. We thank Dra. Rocío Macarena Alonso of CIEMAT for providing an up-to-date land use file of the Madrid Community. We also thank Eugenio Sánchez García of CIEMAT who transformed to ASCII format the urban information existing in CORINE database. Finally, we also thank Dr Mukul Tewari of NCAR for providing the NCEP operational data. This work was funded by the Ministry of Environment of Spain and partially by the project CGL2009-12797-C03-03 (Spanish Ministry of Science and Innovation).

References

Arnfield AJ. 2003. Two decades of urban climate research: A review of turbulence, exchanges of energy and water, and the urban heat island. *International Journal of Climatology* **23**: 1–26.

Bougeault P, Lacarrère P. 1989. Parameterization of orography-induced turbulence in a mesobeta-scale model. *Monthly Weather Review* **117**: 1872–1890.

Chen F, Dudhia J. 2001. Coupling an advanced land-surface/hydrology model with the Penn State/NCAR MM5 modeling system. Part I: Model implementation and sensitivity. *Monsoon Weather Review* **129**: 569–585.

Ching J, Brown M, McPherson T, Burian S, Chen F, Cionco R, Hanna A, Hultgren T, Sailor D, Taha H, Williams D. 2009. National Urban Database and Access Portal Tool. *BAMS* **90**: 1157–1168.

Dudhia J. 1989. Numerical study of convection observed during the winter monsoon experiment using a mesoscale two-dimensional model. *Journal of Atmospheric Science* **46**: 3077–3107.

Hong S-Y, Dudhia J, Chen S-H. 2004. A Revised Approach to Ice Microphysical Processes for the Bulk Parameterization of Clouds and Precipitation. *Monthly Weather Review* **132**: 103–120.

Hu X-M, Nielsen-Gammon JW, Zhang F. 2010. Evaluation of Three Planetary Boundary Layer Schemes in the WRF model. *Journal of Applied Meteorology and Climatology* **49**: 1831–1844.

Janjic ZI. 1994. The step-mountain eta coordinate: Further development of the convection, viscous sublayer, and turbulent closure schemes. *Mons oon Weather Review* **122**: 927–945.

Kanda M, Kawai T, Kanega M, Moriwaki R, Narita K, Hagishima A. 2005. A simple energy balance model for regular building arrays. *Boundary-Layer Meteorology* **116**: 423–443.

Kikegawa Y, Genchi Y, Yoshikado H, Kondo H. 2003. Development of a numerical simulation system toward comprehensive assessments of urban warming countermeasures including their impacts upon the urban buildings energy demands. *Applied Energy* **76**: 449–466.

Kusaka H, Kondo H, Kikegawa Y, Kimura F. 2001. A simple single-layer urban canopy model for atmospheric models: comparison with multi-layer and slab models. *Boundary-layer Meteorology* **101**: 329–358.

Landsberg HE. 1981. *The Urban Climate*. Academic Press: New York, 277.

Lemone MA, Chen F, Tewari M, Dudhia J, Geerts B, Miao Q, Coulter RL, Grossman RL. 2010. Simulating the IHOP_2002 Fair-Weather CBL with the WRF-ARW-Noah Modeling System. Part II: Structures from a Few Kilometers to 100 km across. *Monthly Weather Review* **138**: 745–764.

Lemonsu A, Belair S, Mailhot J. 2009. The New Canadian Urban Modelling System: Evaluation for Two Cases from the joint Urban 2003 Oklahoma City Experiment. *Boundary-Layer Meteorology* **133**: 47–70.

Lo Jeff CF, Lau Alexis KH, Chen F, Fung Jimmy CH, Leung Kenneth KM. 2006. Urban Modification in a Mesoscale Model and the Effects on the Local Circulation in the Pearl River Delta Region. *Journal of Applied Meteorology and Climatology* **46**: 457–476.

Martilli A, Clappier A, Rotach MW. 2002. An urban surface exchange parameterization for mesoscale models. *Boundary-Layer Meteorology* **104**: 261–304.

Martilli A, Roulet Y-A, Junier M, Kirchner F, Rotach MW, Clappier A. 2003. On the impact of urban surface exchange parameterizations on air quality simulations: the Athens case. *Atmospheric Environment* **37**: 4217–4231.

Masson V. 2000. A physically-based scheme for the urban energy budget in atmospheric models. *Boundary-Layer Meteorology* **94**: 357–397.

Mlawer EJ, Taubman SJ, Brown PD, Iacono MJ, Clough SA. 1997. Radiative transfer for inhomogeneous atmospheres: RRTM, a validated correlated-k model for the longwave. *Journal of Geophysical Research* **102**(D14): 16663–16682.

Oke TR. 1987. *Boundary Layer Climate*, 2nd edn, Methuen: London, UK, 435.

Palacios M, Kirchner F, Martilli A, Clappier A, Martín F, Rodríguez ME. 2002. Summer ozone episodes in the Greater Madrid area. Analyzing the ozone response to abatement strategies by modelling. *Atmospheric Environment* **36**: 5323–5333.

Rosenzweig C, Solecki WD, Cox J, Hodges S, Parshall L, Lynn B, Goldberg R, Gaffin S, Slosberg RB, Savio P, Watson M, Dunstan F. 2009. Mitigating New York City's Heat Island: Integrating Stakeholder Perspectives and Scientific Evaluation. *BAMS* **90**: 1297–1312.

Sailor D. 2011. A review of methods for estimating anthropogenic heat and moisture emissions in the urban environment. *International Journal of Climatology* **31**: 189–199.

Saiz S, Kennedy C, Bass B, Pressnail K. 2006. Comparative Life Cycle Assessment of Standard and Green Roofs. *Environmental Science and Technology* **40**: 4312–4316.

Salamanca F, Krpo A, Martilli A, Clappier A. 2010a. A new Building Energy Model coupled with an Urban Canopy Parameterization for urban climate simulations – Part I. Formulation, verification and a

sensitive analysis of the model. *Theoretical and Applied Climatology* **99**: 331–344.

Salamanca F, Martilli A. 2010. A new Building Energy Model coupled with an Urban Canopy Parameterization for urban climate simulations – Part II. Validation with one dimension off-line simulations. *Theoretical and Applied Climatology* **99**:: 345–356.

Salamanca F, Martilli A, Tewari M, Chen F. 2011. A study of the urban boundary layer using different urban parameterizations and high-resolution urban canopy parameters with WRF. *Journal of Applied Meteorology and Climatology* **50**: 1107–1128.

Skamarock WC, Klemp JB, Dudhia J, Gill DO, Barker DM, Duda M, Huang X-Y, Wang W, Powers JG, NCAR Technical Note 2008. A description of the Advanced Research WRF version 3. NCAR Technical Note TN-475+STR, 125.

Sobrino JA, Sòria G, Oltra-Carrió R, Jiménez-Muñoz JC, Romaguera M, Cuenca J, Hidalgo V, Franch B, Mattar C, Julien Y, Bianchi R, Paganini M, Moreno JF, Alonso'L, Fernández-Renau A, Gómez JA, de Miguel E, Gutiérrez Ó, Jiménez M, Prado E, Rodríguez-Cantano R, Ruiz I, Nerry F, Najjar G, Kastendeutch P, Pujadas M, Molero F, Martilli A, Salamanca F, Fernández F, Galán E, Cañada R, Hernández E, Hidalgo J, Acero JÁ, Romero JM, Moya F, Gimeno L. 2009. DESIREX 2008 Final Report Contract n°: 21717/08/I-LG (http://www.uv.es/desirex).

Terradellas E, Cano D. 2007. Implementation of a single-column model for fog and low cloud forecasting at Central-Spanish airports. *Pure and Applied Geophysics* **164**: 1327–1345.

Yagüe C, Zurita E, Martínez A. 1991. Statistical analysis of the Madrid urban heat island. *Atmospheric Environment* **25B**: 327–332.

